

Geophysical Research Letters®



RESEARCH LETTER

10.1029/2023GL104410

Key Points:

- A nonlinearly decayed velocity profile and spontaneous shear localization are observed in plane shear granular flows under high normal stress
- The monotonically decayed granular temperature may lead to inhomogeneities in very dense granular flows and thus to shear localization
- The length scale of the non-local model in very dense granular flows is estimated based on experimental observation

Supporting Information:

Supporting Information may be found in the online version of this article.

Correspondence to:

W. Hu,
huwei1999@126.com

Citation:

Li, Y., Hu, W., Xu, Q., Huang, R., Chang, C., Chen, J., & Wang, Y. (2024). Velocity profile geometries and granular temperature distributions in very dense granular flows. *Geophysical Research Letters*, 51, e2023GL104410. <https://doi.org/10.1029/2023GL104410>

Received 6 MAY 2023
Accepted 22 DEC 2023



Author Contributions:

Conceptualization: Yan Li, Runqiu Huang, Jianye Chen, Yujie Wang
Data curation: ChingShung Chang
Formal analysis: ChingShung Chang
Funding acquisition: Qiang Xu, Runqiu Huang
Methodology: Yan Li, Jianye Chen, Yujie Wang
Software: Yan Li
Supervision: Qiang Xu, Runqiu Huang
Validation: Jianye Chen, Yujie Wang

© 2024. The Authors.

This is an open access article under the terms of the [Creative Commons Attribution-NonCommercial-NoDerivs](https://creativecommons.org/licenses/by-nc-nd/4.0/) License, which permits use and distribution in any medium, provided the original work is properly cited, the use is non-commercial and no modifications or adaptations are made.

Velocity Profile Geometries and Granular Temperature Distributions in Very Dense Granular Flows

Yan Li¹, Wei Hu¹ , Qiang Xu¹, Runqiu Huang¹, ChingShung Chang², Jianye Chen³ , and Yujie Wang^{1,4}

¹State Key Laboratory of Geo-Hazard Prevention and Geo-Environment Protection, Chengdu University of Technology, Chengdu, China, ²Department of Civil Engineering, University of Massachusetts, Amherst, MA, USA, ³State Key Laboratory of Earthquake Dynamics, Institute of Geology, China Earthquake Administration, Beijing, China, ⁴School of Physics and Astronomy, Shanghai Jiao Tong University, Shanghai, China

Abstract Understanding the motion of particles in very dense granular flows is crucial for comprehending the dynamics of many geological phenomena, and advancing our knowledge of granular material physics. We conduct transparent ring shear experiments to directly observe the granular motion under relatively high-pressure conditions, and find that the granular velocity non-linearly decays, forming an approximately 7-particle-diameter-thick localized shear band. A fitting curve underlying non-local physics can be used to well predict velocity profile geometries that are almost independent of normal stress and shear velocity. Moreover, experimental results show monotonically decreasing granular kinetic temperature, which may be caused by energy dissipation due to more inelastic contacts under high confining pressures. The variation of granular temperature will significantly influence the local yield stress and rheological properties, which may lead to inhomogeneous fluidity of the material and thus to shear localization in very dense granular flows.

Plain Language Summary Understanding how particles move under high pressure is essential for studying various geological phenomena and advancing our understanding of granular material physics. In this study, transparent ring shear experiments are conducted to observe the motion of granular particles in very dense granular flows under high normal stress. It is found that the velocity distribution progressively decays and forms a shear band with a width of approximately 7 particle diameters. We suggest an equation that can well predict the velocity profile both of the quasi-linear velocity in the fast-moving shear zone and the exponential velocity curve in the slow-motion region. Furthermore, we analyze the distribution of particle velocity fluctuation and particle density across the sample. Near the moving plate, the particle velocity fluctuation is more intense and the particle density is lower, gradually decreasing far from the moving plate. This phenomenon may be caused by energy dissipation due to inelastic contact between particles. The mechanical properties of the granular material are influenced by these variations in velocity fluctuation and particle density. Thus, this leads to an inhomogeneous shear strain rate and promotes the formation of shear zones under relatively high-pressure conditions.

1. Introduction

Geological processes, including faults, rock avalanches, landslides, and debris flows, all involve very dense granular flows with varying shear velocities (Bagnold, 1954; Fukuoka et al., 2006; Savage & Hutter, 1989). Understanding the dynamics of granular assemblies, particularly under highly confined stress states, is crucial for advancing our knowledge of these geological flows. Numerous experiments have focused on observing granular motion under free-surface and low normal stress conditions (Goyon et al., 2008; Houssais et al., 2015; MiDi, 2004; Savage & Hutter, 1989; Savage & Sayed, 1984; Schall & van Hecke, 2010; Taylor & Brodsky, 2020). Meanwhile, numerical simulations strive to elucidate the principles governing granular motion under high confining pressure conditions (Aharonov & Sparks, 2002; Baran & Kondic, 2005; Y. I. Zhang & Campbell, 1992). Some experiments with natural minerals suggest that shear localization under high-pressure conditions is relevant to grain comminution (Fukuoka et al., 2006, 2007; Rui et al., 2021; Sammis & King, 2007). However, direct observations of ideal granular flows are still necessary to gain further insights into velocity profile distribution and the physical processes involved in shear zone formation under high confining pressures.

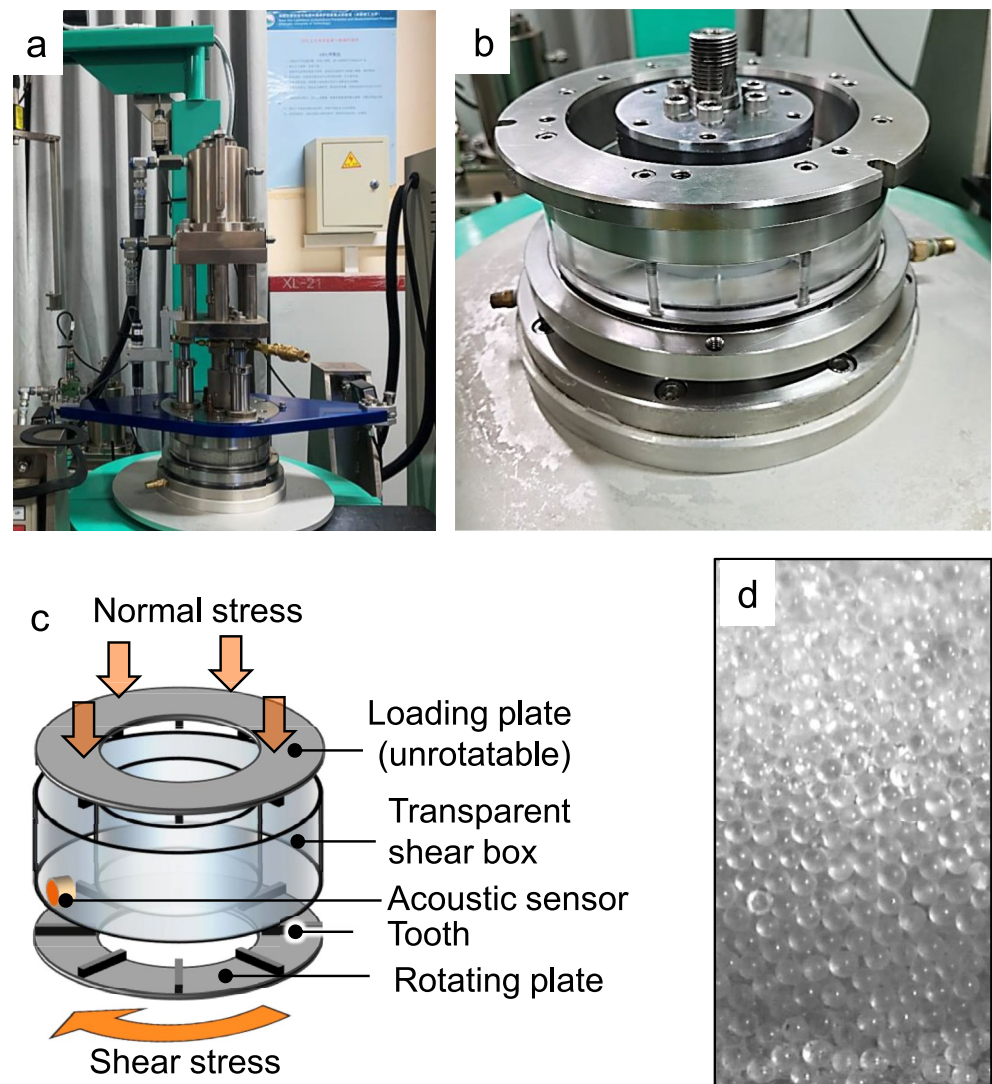


Figure 1. (a) The ICL-2 ring-shear machine and (b) the transparent chamber. (c) The schematic diagram of the apparatus. (d) The particles observed through the transparent side wall.

In this study, we carry out transparent ring-shear experiments to monitor granular motion over varying shear speeds (0.01–0.5 m/s) under relatively high normal stresses, ranging from 0.1 to 0.5 MPa, frequent in many real geological processes. The velocity fluctuation profile and the volume fraction profile are also obtained, equivalent to the granular kinetic temperature (Goldhirsch, 2008) and the Edwards granular temperature (Chang, 2022; Chang & Deng, 2022; Edwards & Oakeshott, 1989), respectively. Using these data, we try to obtain further insights into the granular dynamics under high-pressure conditions.

2. Methods

In this work, we use glass beads as an ideal granular material, which has a simple geometry and is almost crush-resistant, to gain a fundamental understanding of the sheared granular flows. The glass beads used in this work have a diameter of ~ 0.9 mm. The ICL-2 ring shear machine (Figure 1) is employed in this work, with an annular shear box of 10 cm inner diameter, 14.2 cm outer diameter, and a height of 5.2 cm. Eight steel teeth with 3 mm height are fixed on both the top and bottom plate to increase the friction between the plate and the grains. The rotating bottom plate can apply shear deformation on the bottom of the sample to simulate long-distance plane shear (Sassa et al., 2004). A fundamental boundary condition in this study is the controlled shear velocity applied from the bottom rotating plate.

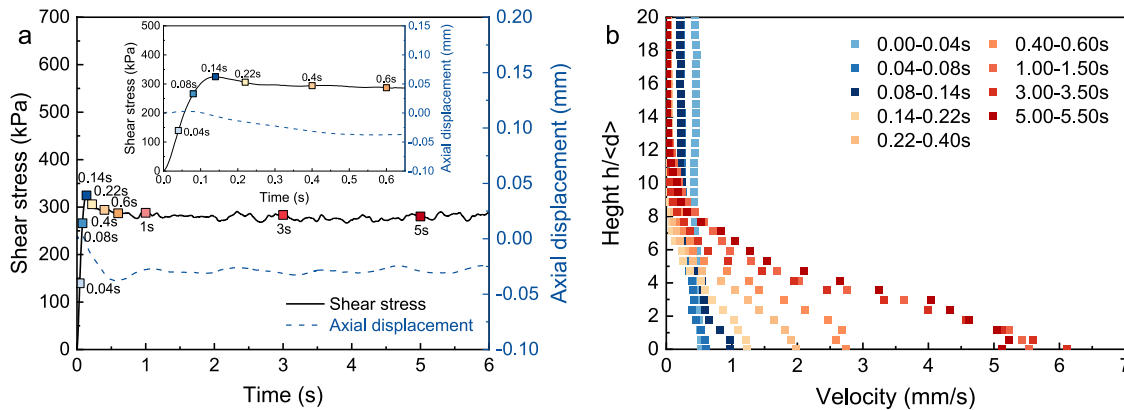


Figure 2. (a) Mechanical data of the ring shear experiments with glass beads. The shear speed is 0.01 m/s, and the normal stress is 0.5 MPa. (b) The evolution of granular velocity distributions are obtained through a particle image velocimetry system.

The shear box sidewall is transparent and made of plexiglass and corundum film, allowing direct observations of the moving particles (see Figure 1d). To capture the images through the transparent chamber, a high-speed camera (Photron, SAZ-MONO) with a macro-lens is used. The shooting frame rate ranges from 250 to 2,000 frames per second (fps), depending on the different shear velocities. The spatial resolution of the images is approximately $0.03d$, where d is the mean particle diameter. The displacement of each grid can be obtained through the comparison between a pair of high-speed images using particle image velocimetry (White et al., 2003). In the monodisperse granular system, the velocity field can be used as a proxy of the granular velocity distribution. Considering the allowable high-speed-shear duration of the apparatus, the lowest resolution velocity is 10^{-4} m/s.

3. Results

We conducted 18 runs of ring shear experiments to shear glass beads at different velocities ranges from 0.01 to 0.5 m/s, under normal stress ranges from 0.1 to 0.5 MPa. A list of the experiments is shown in Table S1 in Supporting Information S1. The gravity stress is found to be only 0.4%–0.08% of the imposed normal stress, which was considered negligible in the experiments.

3.1. Velocity Profile

Figure 2 shows the evolution of the velocity profile during the shear process. At the initiation process (i.e., 0–0.2 s before the yield stress), the sample undergoes full-section shear deformation (as indicated by the blue lines in Figure 2b) and becomes rearranged to its critical volume fraction (particle volume divided by the total volume) to allow continuous flow (da Cruz et al., 2005; MiDi, 2004; van der Elst et al., 2012). The granular flow then reaches a steady state characterized by an almost constant shear resistance and volume. The shear process can be divided into an initiation state and a steady state, as shown in Figure 2. In this work, we focus on the granular motion during the steady state, rather than the complex initiation dynamics. The granular velocity profiles are mostly steady, but with a slight fluctuation around a certain value in the steady state (after 1 s). To filter out high-frequency fluctuations in local velocity measurements, we calculated the average velocity over 1-s intervals (Taylor & Brodsky, 2020). For each layer, we used the mean value of these 1-s bins to obtain the velocity distribution, and assessed the error bar through these binned data.

We present the normalized velocity profiles obtained from all the experiments with varying shear velocities (0.01, 0.05, 0.1, 0.3, and 0.5 m/s) and normal stresses (0.1, 0.2, 0.3, and 0.5 MPa) in Figure 3a. We use dimensionless values, V/V_{\max} (granular velocities normalized by the maximum velocity), and h/d (height normalized by the mean particle diameter), to account for the scaling effect. $h/d = 0$ corresponds to the position of the upper edge of the tooth in the rotating plate. Surprisingly, the normalized velocity profiles for all experiments are very similar, almost independent of the imposed normal stresses and shear velocities. We can separate the granular flows into regions according to the velocity profile. (a) The flow region, the fast-moving layer closest to the moving wall (bottom), exhibits a quasi-linear velocity distribution, similar to the hypothetical linear velocity profile in a

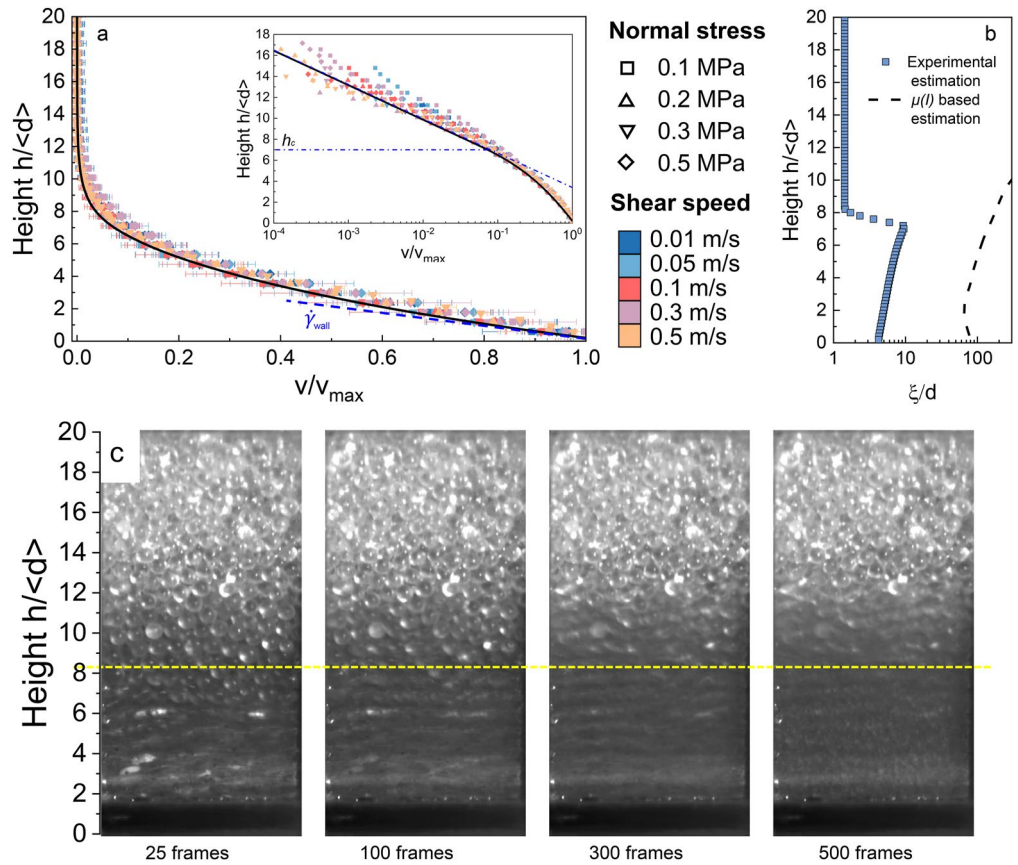


Figure 3. (a) The normalized velocity geometries of glass beads under 0.1–0.5 MPa imposed normal stresses and 0.01–0.5 m/s shear velocities. (inset) The granular velocity will decay exponentially in the creeping region. The solid line shows velocity profiles predicted by the non-local rheology. (b) Estimation of correlation length ξ through the experiments (blue square) and the $\mu(I)$ based model (dash line, Kamrin & Koval, 2012). (c) Resynthesis time-lapse (images overlaying) images of sheared glass beads. The static regime adjacent to the fast-moving layer is not “frozen” but slowly creeps even under relatively high normal stress.

plane shear flow (MiDi, 2004). (b) The quasi-static region in the position far from the moving wall, where $\mu < \mu_s$, particles remain almost static (but with extremely slow creeping, as shown in the semi-log figure in Figure 3 inset) (Bouzid et al., 2013). Averaged over time (time-lapse) indicates that there is a transitional region between the quasi-static and lower flow zones. The particles in the quasi-static layer exhibit intermittent slow motion (Hu et al., 2022; MiDi, 2004), and the mean velocity decays exponentially in depth (Komatsu et al., 2001). In the semi-log figures (inset of Figure 3a), we can approximately identify the bifurcation point where the linear velocity distribution transitions as the boundary between the static region to flow one.

We try to describe the velocity profile according to the non-local fluidity model to rationalize the experimental observation. Granular fluidity considers both local and non-local effects from surrounding grains, which can be presented as Equation 1.

$$g = g_{\text{loc}} + \xi^2 \nabla^2 g \quad (1)$$

where $g = \dot{\gamma}/\mu$ is the granular fluidity, g_{loc} is what the fluidity will be if the rheology is local, and ξ is the correlation length describing the spatial spreading of the plastic activity due to the nonlocal relaxation (Bocquet et al., 2009; Goyon et al., 2008; Kamrin & Koval, 2012).

To predict the velocity profile as the experimental observation, two boundary condition is defined. A first boundary is in the upmost boundary of the sample, where $\partial g/\partial h \cong 0$. A second boundary condition is at the moving surface of the sample, with the boundary granular fluidity of $g_{\text{wall}} = \dot{\gamma}_{\text{wall}}/\mu_{\text{wall}}$. The value of $\dot{\gamma}_{\text{wall}}$ can be directly measured from the velocity profile (Figure 3a), and $\mu_{\text{wall}} \approx 0.6$ according to the experimental results (Figure 2a).

By considering a suitable local granular fluidity and an appropriate correlation length ξ for high confining pressure conditions, the velocity profile can be determined using Equation 1.

In the absence of any non-local effect, the granular fluidity is defined as $g_{\text{loc}} = \dot{\gamma} / \mu_{\text{loc}}$ (Kamrin & Koval, 2012). In the quasi-static region, the shear stress is less than the yield stress, and the local fluidity almost vanishes in the region. While in the flow region with an almost linear velocity profile, the local fluidity is almost homogeneous. We may simply assume that:

$$g_{\text{loc}} = \begin{cases} \dot{\gamma}_{\text{wall}} / \mu_{\text{wall}} & h \leq h_c \\ 0 & h > h_c \end{cases} \quad (2)$$

where $\dot{\gamma}_{\text{wall}}$ is the nearly homogeneous shear strain rate in the shear band and h_c is the characteristic thickness of the shear band. The characteristic thickness h_c can be recognized from the bifurcation from the linear curve in the semi-log figure of Figure 3a, demonstrating the position where the flow shows creeping motion.

Herein, we want to determine the correlation length ξ in the quasi-static region and the fast-moving shear band, respectively. In the quasi-static region, the exponential decay velocity profile in the creeping region can be described as an exponential function 3 (Komatsu et al., 2001):

$$V_x(h) \propto \exp(-h/\xi_c) \quad (3)$$

where $V_x(h)$ is the horizontal granular velocity at height h , and ξ_c is the characteristic length.

With the assumption of the local granular fluidity $g_{\text{loc}} \simeq 0$ in the quasi-static region, as shown in Equation 2. We can obtain the relation of the characteristic length ξ_c and the correlation length ξ using Equations 1 and 3.

$$-\frac{C}{\xi_c} \exp\left(-\frac{h}{\xi_c}\right) = \xi^2 \cdot \left[-\frac{C}{\xi_c^3} \exp\left(-\frac{h}{\xi_c}\right)\right] \quad (4)$$

We can obtain $\xi = \xi_c$ in the quasi-static region using Equation 4. This highlights the potential that the creeping motion in the quasi-static region may well be a kind of non-local behavior (Bocquet et al., 2009) caused by the shear zone with a constant correlation length ξ and vanished local fluidity. The correlation length $\xi = 1.43$ d in the quasi-static region can be directly measured through the slope of the velocity profile in the semi-log coordinate in Figure 3a, and also can be resolved using Equation 1 as shown in Figure 3b. The results from different approaches are almost the same.

In the flow region, we can never directly probe the inherent local fluidity in experiments without the influence of non-local behavior. However, it is suggested that the correlation length is correlated with the shear strain rate, $\xi \propto \dot{\gamma}^{-\alpha}$ in the flow region, and $\alpha = 0.5$ (Picard et al., 2005). Through the back analysis from the velocity profile geometries in Figure 3a, we found that $\xi = b\dot{\gamma}^{-\alpha}$, and $b = 2.1$ can well estimate the distribution of ξ in the flow region. Thus, we can obtain the distribution of correlation length both in the static and the flow regions (see Figure 3b). The velocity profile geometries can be well predicted through the non-local model with the boundary condition and the distribution of ξ , as the solid curve in Figure 3a.

3.2. Velocity Fluctuation Profile

The motion of particles in granular systems can be described using molecular motions from thermodynamics, leading to the development of granular kinetic theory. This theory quantifies granular kinetic energy by characterizing a granular flow in terms of the granular kinetic temperature T . The granular kinetic temperature is defined as follows (Goldhirsch, 2008; Taylor & Brodsky, 2017):

$$T = \left\langle \frac{1}{2} m \delta v^2 \right\rangle \quad (5)$$

where m is the particle mass and δv is the difference between instantaneous velocity and mean flow velocity.

In this work, the glass beads used have almost uniform mass. Therefore, the square of the velocity fluctuation is directly proportional to the granular kinetic temperature, as per Equation 5 in a monodispersed system. Figure 4a

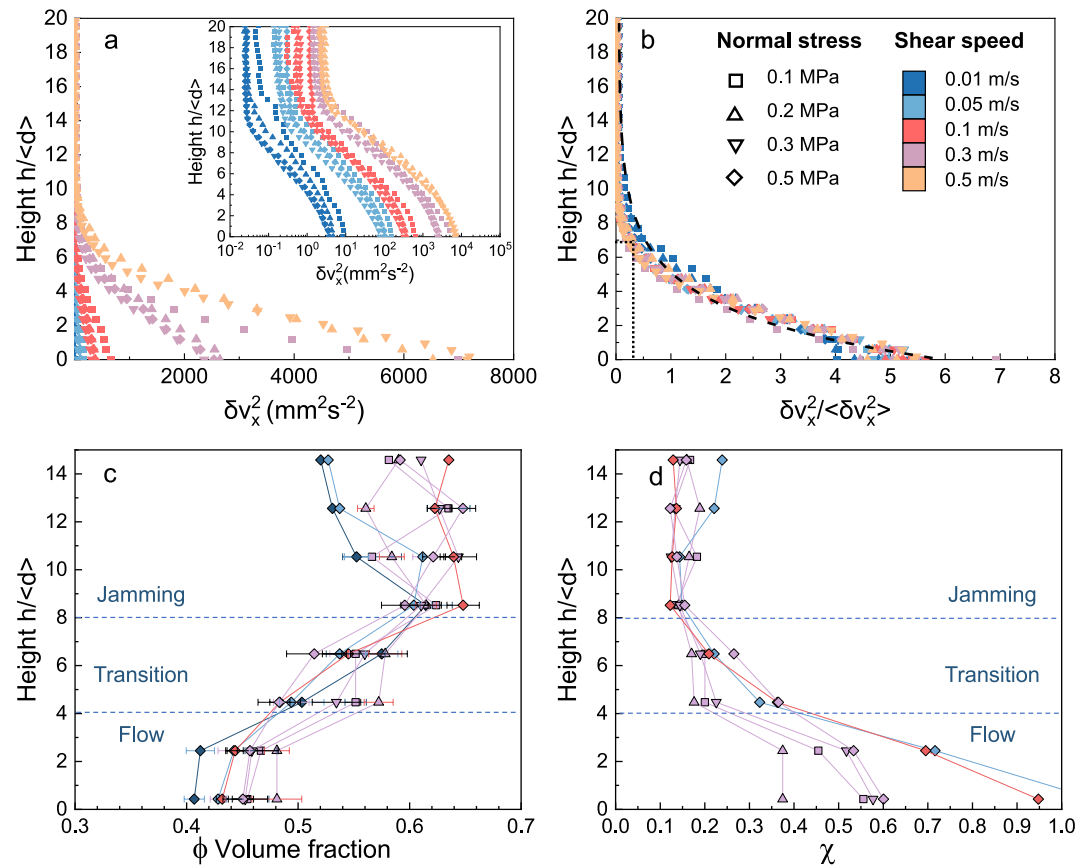


Figure 4. (a) Horizontal velocity fluctuation profiles obtained through the particle image velocimetry system. (inset) The semi-log figure allows detailed observation of the small value. (b) Velocity fluctuations profile normalized by its mean value across the sample. A rough estimation of (c) the volume fraction ϕ through the planar projection and (d) the compactivity χ profile.

presents the horizontal velocity fluctuation profiles in the steady state, obtained by calculating the difference between the instantaneous velocity and the temporal- and spatial-average velocity of the grains in each height. The granular kinetic temperature varies across the entire section and depends on the imposed shear velocity, both in the fast-moving region and in the quasi-static region. This highlights the correlation between the granular kinetic energy and the energy input from the moving wall.

To better illustrate the relative distribution of granular kinetic temperature across the section, the square of velocity fluctuation δv^2 is normalized by its mean value across the sample, as shown in Figure 4b. Interestingly, the normalized velocity profiles for experiments with different shear velocities and normal stresses almost coincide, with an exponential decay from the moving wall. In the quasi-static region, located approximately 7 particle diameters above the moving wall, the granular kinetic temperature almost vanishes.

3.3. Density Profile

The volume fraction, defined as the ratio of granular volume to total volume, is a crucial parameter for describing collective microstructure (MiDi, 2004). In Figure 4c, we present the estimated volume fraction obtained from high-speed images. The sample is divided into multiple 2-mm-thick layers, and the projected area occupied by particles in each layer is used to calculate the 2D projection volume fraction distribution. By using the empirical correlation between 2D and 3D volume fraction suggested by Carleo et al. (2019), we can roughly estimate the volume fraction as shown in Figure 4c. Although there may be inaccuracies in this estimation, we believe that the relative variation tendency of the volume fraction is still meaningful.

The high confining pressure maintains the granular assemblies in a dense flow regime characterized by a network of sustained contacts (MiDi, 2004). The layer adjacent to the moving wall, consisting of 4–5 particles, has a

relatively small but uniform volume fraction, corresponding to the fast-moving layer with a quasi-linear velocity distribution. In contrast, the region far from the moving wall has a much higher volume fraction, resulting in a densely packed structure that causes jamming and keeps the assembly in a quasi-static region. The volume fraction monotonically changes between the flow and jamming regions.

The volume fraction ϕ ranges between $\phi_{\text{RLP}} \approx 0.4$ for the random loose packing (the lowest ϕ observed in the experiments), and $\phi_{\text{RCP}} \approx 0.64$ for the random close packing for ideal spheres. Thus, we can roughly estimate the variation tendency of the Edwards compactivity χ (Edwards & Oakeshott, 1989) according to the relation between χ and ϕ (Chang, 2022; Chang & Deng, 2022; Xia et al., 2015; Yuan et al., 2021), and the result is shown in Figure 4d. The Edwards compactivity represents the dynamic effective temperature of the granular system in the framework of equilibrium statistical physics (Baule et al., 2018; Chang, 2022). Thus, we obtain a rough estimate of the profile of Edwards granular temperature, which is essential for understanding the transition from the quasi-static region to the flow one. Although there may be some inaccuracies in the quantification, the trend we observe is reliable.

4. Discussion

4.1. The Granular Temperature and the Spontaneous Shear Localization

The formation of shear zones in low-pressure plane shear experiments is typically attributed to stress gradients caused by gravity. Within these experiments, the normal stress field varies across the sample due to the overburden pressure $P = P_0 + \rho gh$, where P_0 represents the imposed normal stress. The shear stress field is generally considered uniform in the plane shear configuration. In regions where the shear stress exceeds the yield stress, $\tau > \tau_{\text{yield}} = \mu_s(P_0 + \rho gh)$, the material flows and forms a shear band in the upper layer, where the gravity-induced additional pressure is minimized.

However, under relatively high confining pressure conditions, where the pressure gradient induced by gravity becomes negligible ($P_0 \gg \rho gh$), the normal stress and shear stress fields become almost homogeneous (neglecting stress fluctuations) across the sample due to force equilibrium (Berzi, 2014). The explanation of shear zone formation used in low-pressure yields in the high-pressure plane shear tests. Despite the nearly homogeneous stress field, we discovered a highly inhomogeneous response in shear strain rate, as depicted in Figure 3.

The problem raised here is what mechanisms cause the inhomogeneities in the material? As shown in Figure 4, both velocity fluctuation and packing density vary along the profile. The yield stress and rheological properties of granular material are correlated with granular velocity fluctuation and packing density (Goldhirsch, 2008; Guazzelli & Pouliquen, 2018; Kamrin, 2019; Q. Zhang & Kamrin, 2017). Within the frameworks of kinetic theory and granular thermodynamics, respectively, velocity fluctuation is characterized as granular kinetic temperature, while packing compactivity χ is equivalent to Edwards' granular temperature (Chang, 2022). Under high confining pressure, more inelastic behaviors, such as friction, inelastic collisions, and grain attrition, will consume mechanical energy (Goldhirsch, 2008; Kou et al., 2017) and thus may lead to gradually "cooling" of granular temperature in the athermal granular system. As the granular temperature monotonically decreases with distance from the moving wall (see Figure 4), yield stress and granular fluidity vary accordingly, which may lead to an inhomogeneous shear strain rate and spontaneous shear localization under high-pressure conditions. Both experimental results and previous research consistently indicate that shear zones in dense granular flows typically occur within a specific thickness range of 5–10 particles (Pouliquen & Forterre, 2009; Savage & Hutter, 1989; Siman-Tov & Brodsky, 2021).

4.2. The Correlation Length ξ in Very Dense Granular Flows

The grain motion and microstructure rearrangement will influence the material over some grain-size-dependent correlation length ξ (Kamrin, 2019). Under the free surface and low confining pressure conditions, the $\mu(I)$ based model is widely used to estimate ξ through the difference or the ratio of μ and μ_s , and discussed in predicting the velocity profiles (Bouzid et al., 2013; Kamrin, 2019; Kamrin & Koval, 2012). However, under a moderate/high confining pressure, the inertial number $I = \dot{\gamma}d / \sqrt{P/\rho_s}$ is extremely small, on the order of $\sim 10^{-3}$ – 10^{-5} in our experiments, resulting in nonphysically large values of ξ up to several tens or even hundreds of particle diameters (dash line in Figure 3b, detailed in Text S2 in Supporting Information S1). Therefore, properly estimating correlation length in very dense granular flow remains challenging.

As shown in Figure 3b, we measured the distribution of ξ under relatively high normal stress conditions. Both the scales and the distribution of ξ are analogous to that in low confining pressure conditions: a higher value of ξ up to 10 particle diameters near the jamming transition, and will decrease and converge to a low value on both sides of that point. In the static region, the value $\xi \approx 1.43$ d is similar to many free surface or low confining pressure experiments, approximately 1–1.5 d (Crassous et al., 2008; Jain et al., 2002; Komatsu et al., 2001; Mikkelsen, 2005). However, the specific value of ξ in the static region is sensitive to material characteristics, such as approximately 4.9 d for painted glass beads, and 2–2.5 d for steel beads (Bonamy et al., 2002; Jain et al., 2002).

Near the jamming transition, where the granular packing is dense and particle motion remains obvious, local behavior can significantly influence particle motion within several particle diameters, resulting in a higher ξ . However, in fast-moving shear zones, dynamic dilation leads to a decrease in packing density, possibly causing a decrease in ξ due to the decrease of intergranular contacts. Nevertheless, experimental results demonstrate that ξ remains within several particle diameters despite the relatively high confining pressure.

4.3. Implications

Directly observing velocity distribution and shear zone formation in ideal granular materials under high confining pressures is of broad interest in geosciences and granular physics. Experimental results demonstrate that after a transition phase, the shear strain will localize within a shear zone with several particle-diameter thick during the steady state. This physical phenomenon presented here enhances our understanding of fundamental mechanisms involved in shear zone localization during mass wasting processes such as landslides, avalanches, and debris flows, as well as faults, despite the inherent complexity of natural conditions (Sammis & King, 2007). Experimental results also demonstrate that the overburden pressure and shear velocity may have very limited influence on the shear zone thickness, at least in the condition within the experiments (see Figure 3a, confining pressures ranging 0.1–0.5 MPa and shear velocities ranging 0.01–0.5 m/s). However, the formation of shear zones in natural settings can be much more complex and influenced by various factors, including (but not limited to) mineral compositions, geological processes, particle comminutions, and the complicated grain size distribution (Fukuoka et al., 2006, 2007; Rui et al., 2021). Meanwhile, these findings shed light on the non-local effects and their length scales under high-pressure conditions. This insight has the potential to advance our ability to accurately estimate both landslide fluidity and shear zone deformation in various geological processes.

4.4. Limitations

The velocity of the central particles cannot be directly measured in this study, as we only observe the outermost particles. Moreover, the additional friction caused by the sidewalls will influence the granular motion of the outermost particles. While this inevitable sidewall friction may have impacted the quantitative outcomes, but likely do not change the trend of the experimental observations. The non-linear velocity distribution and shear localization should still exist in very dense granular flows under high normal stress conditions, regardless of the specific boundary conditions. This is further supported by numerous natural phenomena exhibiting similar shear localization behaviors. The volume fraction distribution measurement shown in Figure 4 is semi-manually assisted, and the values are converted from 2D to 3D, which may have introduced some inaccuracies. Nevertheless, the relative tendency can still be considered reliable and meaningful.

5. Conclusion

The transparent ring shear experiments conducted in this study provide insights into the dynamics of granular materials under high normal stress. The experiment demonstrated that the velocity distribution in sheared granular flows progressively decays and spontaneously forms a shear band. The velocity profile geometries are found to be independent of both velocity and stress under the experimental conditions, including confining pressures ranging 0.1–0.5 MPa and shear velocities ranging 0.01–0.5 m/s. The velocity profiles can be well-fitted by a master curve underlying the non-local physics. Moreover, the experiments show a monotonically decrease in both granular kinetic temperature and Edwards granular temperature, which may be caused by energy dissipation due to inelastic intergranular contacts. The variation in granular temperature may influence local yield stress and rheological properties, and cause inhomogeneities in very dense granular flows, resulting in spontaneous shear localization.

Data Availability Statement

All the original data used in this work can be retrieved from the data set available through (Li, 2023).

Acknowledgments

We are supported by the NSFC for Distinguished Young Scholars of China (42325703) and the National Basic Research Program of China: basic research fund (42090051) and (42107205).

References

- Aharonov, E., & Sparks, D. (2002). Shear profiles and localization in simulations of granular materials. *Physical Review E - Statistical Physics, Plasmas, Fluids, and Related Interdisciplinary Topics*, 65(5), 12. <https://doi.org/10.1103/PhysRevE.65.051302>
- Bagnold, R. A. (1954). Experiments on a gravity-free dispersion of large solid spheres in a Newtonian fluid under shear. *Proceedings of the Royal Society of London. Mathematical and Physical Sciences*, 225, 49–63.
- Baran, O., & Kondic, L. (2005). Velocity profiles, stresses, and Bagnold scaling of sheared granular system in zero gravity. *Physics of Fluids*, 17(7), 1–15. <https://doi.org/10.1063/1.1951567>
- Baule, A., Morone, F., Herrmann, H. J., & Makse, H. A. (2018). Edwards statistical mechanics for jammed granular matter. *Reviews of Modern Physics*, 90(1), 015006. <https://doi.org/10.1103/RevModPhys.90.015006>
- Berzi, D. (2014). Extended kinetic theory applied to dense, granular, simple shear flows. *Acta Mechanica*, 225(8), 2191–2198. <https://doi.org/10.1007/s00707-014-1125-1>
- Bocquet, L., Colin, A., & Ajdari, A. (2009). Kinetic theory of plastic flow in soft glassy materials. *Physical Review Letters*, 103(3), 036001. <https://doi.org/10.1103/PhysRevLett.103.036001>
- Bonamy, D., Daviaud, F., & Laurent, L. (2002). Experimental study of granular surface flows via a fast camera: A continuous description. *Physics of Fluids*, 14(5), 1666–1673. <https://doi.org/10.1063/1.1459720>
- Bouziid, M., Trulsson, M., Claudin, P., Clément, E., & Andreotti, B. (2013). Nonlocal rheology of granular flows across yield conditions. *Physical Review Letters*, 111(23), 238301. <https://doi.org/10.1103/PhysRevLett.111.238301>
- Carleo, L., Sarno, L., Papa, M. N., Tai, Y. C., & Villani, P. (2019). Volume fraction and velocity fields of nearly uniform granular flows in a narrow channel geometry with smooth bed. *Advanced Powder Technology*, 30(10), 2379–2395. <https://doi.org/10.1016/j.appt.2019.07.021>
- Chang, C. S. (2022). Jamming density and volume-potential of a bi-dispersed granular system. *Geophysical Research Letters*, 49(13), e2022GL098678. <https://doi.org/10.1029/2022GL098678>
- Chang, C. S., & Deng, Y. (2022). Compaction of bi-dispersed granular packing: Analogy with chemical thermodynamics. *Granular Matter*, 24(2), 58. <https://doi.org/10.1007/s10035-022-01219-5>
- Crassous, J., Metayer, J. F., Richard, P., & Laroche, C. (2008). Experimental study of a creeping granular flow at very low velocity. *Journal of Statistical Mechanics: Theory and Experiment*, 2008(3), P03009. <https://doi.org/10.1088/1742-5468/2008/03/P03009>
- da Cruz, F., Emam, S., Prochnow, M., Roux, J. N., & Chevoir, F. (2005). Rheophysics of dense granular materials: Discrete simulation of plane shear flows. *Physical Review E - Statistical, Nonlinear and Soft Matter Physics*, 72(2), 1–17. <https://doi.org/10.1103/PhysRevE.72.021309>
- Edwards, S. F., & Oakeshott, R. B. S. (1989). Theory of powders. *Physica A*, 157(3), 1080–1090. [https://doi.org/10.1016/0378-4371\(89\)90034-4](https://doi.org/10.1016/0378-4371(89)90034-4)
- Fukuoka, H., Sassa, K., & Wang, G. (2007). Influence of shear speed and normal stress on the shear behavior and shear zone structure of granular materials in naturally drained ring shear tests. *Landslides*, 4(1), 63–74. <https://doi.org/10.1007/s10346-006-0053-0>
- Fukuoka, H., Sassa, K., Wang, G., & Sasaki, R. (2006). Observation of shear zone development in ring-shear apparatus with a transparent shear box. *Landslides*, 3(3), 239–251. <https://doi.org/10.1007/s10346-006-0043-2>
- Goldhirsch, I. (2008). Introduction to granular temperature. *Powder Technology*, 182(2), 130–136. <https://doi.org/10.1016/j.powtec.2007.12.002>
- Goyon, J., Colin, A., Ovarlez, G., Ajdari, A., & Bocquet, L. (2008). Spatial cooperativity in soft glassy flows. *Nature*, 454(7200), 84–87. <https://doi.org/10.1038/nature07026>
- Guazzelli, É., & Pouliquen, O. (2018). Rheology of dense granular suspensions. *Journal of Fluid Mechanics*, 852, P1. <https://doi.org/10.1017/jfm.2018.548>
- Houssais, M., Ortiz, C. P., Durian, D. J., & Jerolmack, D. J. (2015). Onset of sediment transport is a continuous transition driven by fluid shear and granular creep. *Nature Communications*, 6(1), 6527. <https://doi.org/10.1038/ncomms7527>
- Hu, W., Li, Y., Xu, Q., Huang, R., McSaveney, M., Wang, G., et al. (2022). Flowslide high fluidity induced by shear-thinning. *Journal of Geophysical Research: Solid Earth*, 127(12), e2022JB024615. <https://doi.org/10.1029/2022JB024615>
- Jain, N., Ottino, J., & Lueptow, R. (2002). An experimental study of the flowing granular layer in a rotating tumbler. *Physics of Fluids*, 14(2), 572–582. <https://doi.org/10.1063/1.1431244>
- Kamrin, K. (2019). Non-locality in granular flow: Phenomenology and modeling approaches. *Frontiers in Physics*, 7, 116. <https://doi.org/10.3389/fphy.2019.00116>
- Kamrin, K., & Koval, G. (2012). Nonlocal constitutive relation for steady granular flow. *Physical Review Letters*, 108(17), 178301. <https://doi.org/10.1103/PhysRevLett.108.178301>
- Komatsu, T. S., Inagaki, S., Nakagawa, N., & Nasuno, S. (2001). Creep motion in a granular pile exhibiting steady surface flow. *Physical Review Letters*, 86(9), 1757–1760. <https://doi.org/10.1103/PhysRevLett.86.1757>
- Kou, B., Cao, Y., Li, J., Xia, C., Li, Z., Dong, H., et al. (2017). Granular materials flow like complex fluids. *Nature*, 551(7680), 360–363. <https://doi.org/10.1038/nature24062>
- Li, Y. (2023). Velocity profile geometries and granular temperature distributions in very dense granular flows [Dataset]. figshare. <https://doi.org/10.6084/m9.figshare.22698775.v1>
- MiDi, G. D. R. (2004). On dense granular flows. *European Physical Journal E*, 14(4), 341–365. <https://doi.org/10.1140/epje/i2003-10153-0>
- Mikkelsen, R. (2005). *Granular dynamics: Clustering and shear flows*. PhD thesis. Univ. Twente.
- Picard, G., Ajdari, A., Lequeux, F., & Bocquet, L. (2005). Slow flows of yield stress fluids: Complex spatiotemporal behavior within a simple elastoplastic model. *Physical Review E - Statistical, Nonlinear and Soft Matter Physics*, 71(1), 010501. <https://doi.org/10.1103/PhysRevE.71.010501>
- Pouliquen, O., & Forterre, Y. (2009). A non-local rheology for dense granular flows. *Philosophical Transactions of the Royal Society A: Mathematical, Physical & Engineering Sciences*, 367(1909), 5091–5107. <https://doi.org/10.1098/rsta.2009.0171>
- Rui, S., Wang, L., Guo, Z., Cheng, X., & Wu, B. (2021). Monotonic behavior of interface shear between carbonate sands and steel. *Acta Geotechnica*, 16(1), 167–187. <https://doi.org/10.1007/s11440-020-00987-9>
- Sammis, C. G., & King, G. C. P. (2007). Mechanical origin of power law scaling in fault zone rock. *Geophysical Research Letters*, 34(4), L04312. <https://doi.org/10.1029/2006GL028548>
- Sassa, K., Fukuoka, H., Wang, G., & Ishikawa, N. (2004). Undrained dynamic-loading ring-shear apparatus and its application to landslide dynamics. *Landslides*, 1(1), 7–19. <https://doi.org/10.1007/s10346-003-0004-y>

- Savage, S. B., & Hutter, K. (1989). The motion of a finite mass of granular material down a rough incline. *Journal of Fluid Mechanics*, 199(2697), 177–215. <https://doi.org/10.1017/S0022112089000340>
- Savage, S. B., & Sayed, M. (1984). Stresses developed by dry cohesionless granular materials sheared in an annular shear cell. *Journal of Fluid Mechanics*, 142, 391–430. <https://doi.org/10.1017/s0022112084001166>
- Schall, P., & van Hecke, M. (2010). Shear bands in matter with granularity. *Annual Review of Fluid Mechanics*, 42(1), 67–88. <https://doi.org/10.1146/annurev-fluid-121108-145544>
- Siman-Tov, S., & Brodsky, E. E. (2021). Distinguishing between rheophysical regimes of fluid-saturated granular-flows using dilatancy and acoustic emission measurements. *Granular Matter*, 23(2), 1–11. <https://doi.org/10.1007/s10035-021-01103-8>
- Taylor, S. E., & Brodsky, E. E. (2017). Granular temperature measured experimentally in a shear flow by acoustic energy. *Physical Review E*, 96(3), 032913. <https://doi.org/10.1103/PhysRevE.96.032913>
- Taylor, S. E., & Brodsky, E. E. (2020). Reversible compaction in sheared granular flows and its significance for nonlocal rheology. *Geophysical Research Letters*, 47(10), e2020GL087137. <https://doi.org/10.1029/2020GL087137>
- van der Elst, N. J., Brodsky, E. E., le Bas, P. Y., & Johnson, P. A. (2012). Auto-acoustic compaction in steady shear flows: Experimental evidence for suppression of shear dilatancy by internal acoustic vibration. *Journal of Geophysical Research*, 117(9), B09314. <https://doi.org/10.1029/2011JB008897>
- White, D. J., Take, W. A., & Bolton, M. D. (2003). Soil deformation measurement using particle image velocimetry (PIV) and photogrammetry. *Géotechnique*, 53(7), 619–631. <https://doi.org/10.1680/geot.2003.53.7.619>
- Xia, C., Li, J., Cao, Y., Kou, B., Xiao, X., Fezzaa, K., et al. (2015). The structural origin of the hard-sphere glass transition in granular packing. *Nature Communications*, 6(1), 8409. <https://doi.org/10.1038/ncomms9409>
- Yuan, Y., Xing, Y., Zheng, J., Li, Z., Yuan, H., Zhang, S., et al. (2021). Experimental test of the Edwards volume ensemble for tapped granular packings. *Physical Review Letters*, 127(1), 018002. <https://doi.org/10.1103/PhysRevLett.127.018002>
- Zhang, Q., & Kamrin, K. (2017). Microscopic description of the granular fluidity field in nonlocal flow modeling. *Physical Review Letters*, 118(5), 058001. <https://doi.org/10.1103/PhysRevLett.118.058001>
- Zhang, Y. I., & Campbell, C. S. (1992). The interface between fluid-like and solid-like behaviour in two-dimensional granular flows. *Journal of Fluid Mechanics*, 237, 541–568. <https://doi.org/10.1017/s0022112092003525>

References From the Supporting Information

- Kee, B. L., & Baumann, R. L. (2014). Heat transfer and temperature distribution in a 74 Fin. Retrieved from <http://demonstrations.wolfram.com/HeatTransferAndTemperatureDistributionInAFin/>